DOI: 10.13009/EUCASS2019-251

DOI: ADD DOINUMBER HERE

3D Conjugate Heat Transfer Analysis of a 100 kN Class Liquid Rocket Combustion Chamber

Daniel Eiringhaus[⋆,†]*, Hendrik Riedmann*[⋆]*, Oliver Knab*[⋆] *and Oskar J. Haidn*[‡]
[⋆]*ArianeGroup GmbH*
Robert-Koch-Straße 1, 82024 Taufkirchen
[‡]*Institute of Turbomachinery and Flight Propulsion (LTF), Technische Universität München (TUM)*
Boltzmannstr. 15, 85748 Garching, Germany
daniel.eiringhaus@ariane.group
[†]Corresponding author

Abstract

In order to cut the development costs of liquid rocket engines full-scale hardware tests are supplemented with numerical analyses. For the correct prediction of the engine performance as well as its thermo-mechanical verification conjugate heat transfer analyses are performed. The present work presents ArianeGroup Ottobrunn's novel, fully three-dimensional approach for these investigations and includes first results of such a simulation of a full-scale demonstrator defined in the German national research programme Sonderforschungsbereich Transregio 40.

1. Introduction

During recent years the commercial space launch business has experienced the emergence of new privately funded companies such as SpaceX, Blue Origin and Rocket Lab.

In order to stay competitive in this changing market new disruptive concepts are necessary. In the frame of the European Future Launchers Preparatory Programme (FLPP) ArianeGroup is evaluating concepts like a methane fueled launcher using the Prometheus engine[26] and advanced upper stage engine concepts as demonstrated with the expander cycle technology integrated demonstrator (ETID)[8]. One way to cut the costs during the development process of liquid rocket engines (LRE) is to support the test activities with numerical simulation tools. Once well calibrated, these tools can complement the results of full-scale hardware tests with additional insights in areas that are not accessible to measurements. Furthermore, numerical analyses can offer a much higher spatial resolution of information compared to the strongly localized information obtained from experimental instrumentation.

During the development process of a LRE the prediction of the engine performance and stability as well as the thermo-mechanical verification of the combustion chamber structural integrity and the required life are major objectives. To obtain the necessary information a conjugate heat transfer (CHT) analysis, i.e. a coupled investigation of the combustion process, the thermal conduction in the combustion chamber wall and the coolant flow in the cooling channels of the combustion chamber is required. Similar analyses have been performed e.g. by Negishi et al. [18] and Sharma et al.[24].

In the following section 2 an overview of the established industrial methods for CHT analyses at ArianeGroup Ottobrunn is given. Subsequently, the new methodology for fully resolved 3D CHT investigations is presented. The test case, a virtual full-scale thrust chamber demonstrator defined within the framework of the German national research program Sonderforschungsbereich Transregio 40 (SFB-TRR 40) is outlined. The numerical model of this demonstrator and results of the CHT simulation are presented in section 5. Finally, an outlook on future work is given.

2. Overview of Industrial Conjugate Heat Transfer Tools

An overview of the computational domain of a generic conjugate heat transfer analysis for a typical combustion chamber configuration is given in Figure 1. Three main domains can be differentiated:

- The domain of the combustion Ω_C where the mixing process of the propellants, their reaction, the resulting heat release and the flow of the hot gas have to be modeled.

DOI: 10.13009/EUCASS2019-251

- The domain of the heat conduction in the combustion chamber's structure Ω_S. For typical combustion chambers that are manufactured using an integral high conductivity liner (e.g. copper alloys) with milled cooling channels and a galvanically applied outer shell of materials with high tensile strength (e.g. nickel alloys) two separate structure domains $\Omega_{S,Cu}$ and $\Omega_{S,Ni}$ can be identified. For such a configuration heat transfer between those two domains can be regarded as perfect.

- The domain of the coolant fluid Ω_F where coolant flow including the pressure drop, temperature increase and in some cases the phase change have to be modeled.

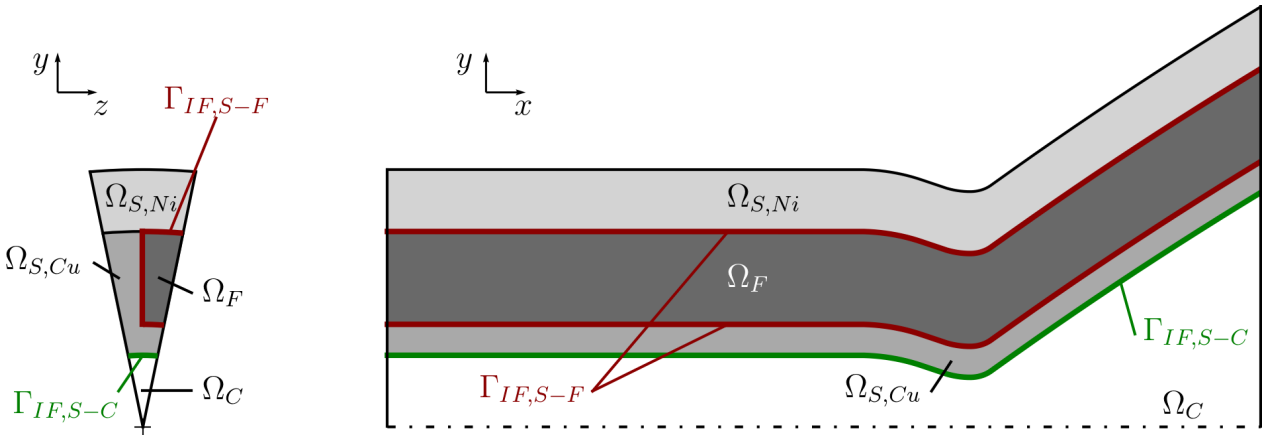

Figure 1: Domains of a Conjugate Heat Transfer analysis

The interfaces between the respective domains, i.e. their common surfaces, are indicated in Figure 1 as $\Gamma_{IF,S-F}$ and $\Gamma_{IF,S-C}$. At the interface surface $\Gamma_{IF,S-F}$ the coolant domain Ω_F and the structure domain Ω_S have to satisfy the coupling condition

$$\dot{q}_S(\Gamma_{IF,S-F}) = -\dot{q}_F(\Gamma_{IF,S-F}). \tag{1}$$

Equally, at the interface surface $\Gamma_{IF,S-C}$ the combustion domain Ω_C and the structure domain Ω_S have to satisfy the coupling condition

$$\dot{q}_C(\Gamma_{IF,S-C}) = -\dot{q}_S(\Gamma_{IF,S-C}). \tag{2}$$

Conjugate heat transfer investigations can be performed at different levels of fidelity as summarized in Table 1. At ArianeGroup Ottobrunn two approaches are established for steady-state CHT analyses of LRE combustion chambers that are used dependent on the required fidelity as well as the desired computational time.

Table 1: Overview of different levels of fidelity for CHT analyses.

domain / coupling	1D	2D	3D
Ω_C	equilibrium chemistry	axisymmetric combustion analysis (CFD)	fully resolved 3D combustion analysis (CFD)
$\Omega_C \leftrightarrow \Omega_S$	Nu-correlations	modeled by CFD	modeled by CFD
Ω_S	radial conduction (e.g. plate)	2D axisymmetric model with radial & axial conduction	fully resolved 3D thermal conduction model (e.g. FEM / FV)
$\Omega_S \leftrightarrow \Omega_F$	Nu-correlations	modeled by CFD	modeled by CFD
Ω_F	1D flow with pressure loss-correlations	(axisymmetric) 3D analysis of single channel	fully resolved 3D CFD

DOI: 10.13009/EUCASS2019-251

2.1 RCFS-II

For quick assessments during early development phases the in-house engineering tool RCFS-II is used. RCFS-II is based on the assumption of chemical equilibrium for the combustion domain (Ω_C) and uses the well established Gordon-McBride code [15, 16] to obtain a 1D profile for hot gas transport properties, composition, temperature and pressure. Heat transfer between the hot gas flow (Ω_C) and the combustion chamber wall (Ω_S) is modeled with Nusselt-type correlations that are based on extensive experimental data. The heat conduction in the combustion chamber wall (Ω_S) can be modeled with either a 1D plate model including an analytic fin model or with a 2D finite element model (FEM). The coolant flow in the cooling channels (Ω_F) is modeled with 1D pipe flow correlations for pressure and velocity. Again, the heat transfer between the solid (Ω_S) and the fluid domain (Ω_F) is modeled with Nusselt-correlations tailored for this specific application that are based on a vast heritage of experimental data. A detailed description of RCFS-II and its advanced features is given by Fröhlich et al.[7] and Mäding et al.[14].

2.2 Rocflam-II / CFX

For detailed investigations of full-scale hardware computational fluid dynamics (CFD) tools are applied for the simulation of the turbulent combustion process and the coolant flow. Combustion simulations are carried out with the in-house CFD tool Rocflam-II that has been developed, applied and improved by ArianeGroup Ottobrunn for over 20 years. Rocflam-II is a 2D axisymmetric spray combustion code that solves the Favre-averaged Navier Stokes equations. Several dedicated modules for the simulation of LRE are included such as a Lagrangian module for liquid propellant injection including the evaporation model of Abramzon and Sirignano [1], a module for liquid coolant films and different combustion models. A detailed description of Rocflam-II and exemplary applications are given by Frey et al.[6].

The computations for both the coolant flow (Ω_F) and the heat conduction in the combustion chamber structure (Ω_S) are performed with the commercial tool Ansys CFX. For the coolant flow the Reynolds Averaged Navier Stokes (RANS) equations are solved. Turbulence is modeled with Menter's k-ω-SST model[17] and wall roughness in the cooling channels is considered where necessary. Special attention is given to the properties of the coolant medium and tabulated real gas data from the NIST database[13] and the GASPAK package are used. For the temperature field in the structure domain Ω_S the energy equation is solved by Ansys CFX using its finite volume method. The coolant (Ω_F) and the structure domain (Ω_S) of the simulation are directly coupled by Ansys CFX by ensuring heat flux conservation between both domains, thus equation 1 is satisfied. The typical computational domain is illustrated in Figure 1 and is comprised of half a channel in the coolant domain and half a fin plus the upper and lower wall above the cooling channel in the structure domain.

For the coupling between the combustion domain (Ω_C) and the wall structure domain (Ω_S) a loose coupling approach is used. At the interface surface $\Gamma_{IF,S-C}$ both domains require a boundary condition. For the combustion domain Ω_C a wall temperature, i.e. a Dirichlet boundary condition is prescribed. For the solid domain Ω_S the heat flux, i.e. a Neumann boundary condition is used. For both domains the value of the boundary condition depends on the solution of the other domain. Thus, the conjugate problem can only be solved iteratively and Rocflam-II and Ansys CFX have to be run alternately and their boundary conditions updated in each coupling iteration step. When both the solution of the wall temperature and the resulting hot gas heat flux converge, the heat flux conservation at the interface (equation 2) is satisfied. This coupling process is illustrated in Figure 2.

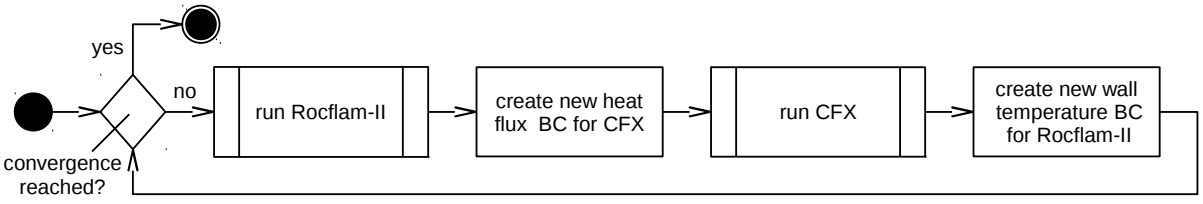

Figure 2: Coupling of Rocflam-II and CFX

As in this case a 2D axisymmetric simulation of the hot gas domain is coupled with a 3D simulation for the structure and the coolant flow domain some processing of the boundary condition data is required. The 2D wall temperature profile from Ansys CFX has to be averaged in circumferential direction whereas the wall heat flux profile obtained from Rocflam-II is only 1D and thus represents a circumferential mean value.

DOI: 10.13009/EUCASS2019-251

3. Fully-Resolved 3D Conjugate Heat Transfer Method

The methods presented in section 2 do not resolve circumferential variations in the hot gas domain that can result e.g. from the injection element pattern. To resolve this circumferential stratification a 3D analysis of the combustion process is necessary. As this analysis can lead to significant wall heat flux variations in circumferential directions a coupling to a single cooling channel / fin pair is not sufficient and a matching domain of the structure and coolant flow has to be modeled. This approach offers the highest fidelity at the drawback of increased computational efforts, thus it complements the previously described methods rather than replacing them.

The general coupling procedure follows the same steps as described for the 2D axisymmetric coupling of Rocflam-II and Ansys CFX as illustrated in Figure 2. Computations for the combustion simulation are carried out with Rocflam-II's successor code Rocflam3 that is described in more detail in the following section 3.1. The simulation of the structure and coolant flow domain is again performed with Ansys CFX however the domain size is significantly increased in circumferential direction.

3.1 Combustion - Rocflam3

Based on more than 20 years experience with the 2D in-house tool Rocflam-II a successor version, namely Rocflam3, is being developed in recent years. Rocflam3 offers the full 3D capabilities while including all the modules of its previous versions that are vital for the comprehensive simulation of LRE thrust chambers. Rocflam3 solves the Favre averaged Navier-Stokes equations in three spatial dimensions. The conservation equations for mass, momentum and enthalpy are discretized with a Finite Volume scheme utilizing the SIMPLE algorithm as described by Patankar and Spalding [19]. The resulting system of partial differential equations is solved using Stone's strongly implicit procedure [27].

In addition to a mass flow inlet, propellant injection of liquid or liquid-like transcritical propellants like e.g. liquid oxygen or storable propellants like hydrazine a Lagrangian module is available. The Lagrangian module allows the simulation of the droplet trajectories and their evaporation and is loosely coupled to the Eulerian flow solver. The computational effort is reduced by limiting the amount of tracked particles to a number of representative droplet parcels. Each parcel is characterized by a discrete diameter, injection angle and velocity. The vaporization of the droplet parcels is modeled using the correlations of Abramzon and Sirignano [1]. Along its trajectory each droplet parcel interacts with the Eulerian phase through mass, momentum and source terms in the conservation equations in the continuous phase. Droplet motion and evaporation in turn is dependent on the surrounding continuum. However, displacement effects of the droplets in the Eulerian phase and droplet-droplet interaction are not modeled.

Turbulence modeling in Rocflam3 can be done with several two-equation turbulence models. Next to the k-ε-model of Launder and Sharma [12], the two-layer-model of Rodi [23] and Wilcox's k-ω model [28] that are also included in Rocflam-II the widely spread and well accepted k-ω-SST model of Menter [17] is implemented. Wall roughness models on the hot gas wall can be considered in Rodi's two-layer-model, Wilcox's k-ω model and Menter's k-ω-SST model. For the rough wall treatment in the SST model the approach described by Aupoix [3] is implemented in Rocflam3. Successful application of the roughness model was demonstrated by the authors for a full-scale test case in Eiringhaus et al. [5].

Several approaches for the modeling of the combustion process of the propellants are available in Rocflam3. For hypergolic propellant combinations a skeletal chemistry approach is used that is based on the extensive experience with Rocflam-II and its predecessors and described in detail by Knab et al. [11]. For the combustion of hydrogen and oxygen the chemical timescale τ_{chem} is significantly lower than the turbulent timescale τ_{turb} yielding a high Damköhler Number

$$Da = \frac{\tau_{\text{turb}}}{\tau_{\text{chem}}} \tag{3}$$

and thus allowing the assumption of chemical equilibrium. Hence, the combustion process is modeled using an equilibrium-based pPDF (presumed probability density function) chemistry model. The interaction of turbulence and combustion is taken into account by a presumed β-PDF. In addition to the governing equations of a non-reacting flow, transport equations for mixture fraction and its variance have to be solved. All necessary fluid and transport properties and the temperature and species composition are tabulated over mixture fraction, mixture fraction variance, enthalpy and pressure beforehand. Furthermore, a non-adiabatic flamelet model is being developed in-house by Rahn [21] to complement the equilibrium based approach with an efficient tabulated chemistry model for propellant combinations where the assumption of equilibrium does not hold.

Rocflam3 uses block-structured grids that do not resolve individual injection elements by grid edges or O-grids. Instead, if a mass flow inlet is specified oxidizer and fuel inlet boundary conditions are mapped to cells whose center of area is within the circle defining the injection area. This approach ensures a high flexibility during the design process

DOI: 10.13009/EUCASS2019-251

as a single grid can be used to investigate different injector configurations. The resulting error in injection impulse and velocity depends on the grid resolution but is in general below 1%.

In recent works Rocflam3 has been applied to and validated against well-instrumented lab- and sub-scale experiments. Both H2/O2 and CH4/O2, currently the propellant combinations of greatest interest for European launcher propulsion application, have been investigated. Both the results of an axisymmetric and a 3D simulation with Rocflam3 carried out by Riedmann et al. [22] for a 19 element H2/O2 sub-scale combustion chamber showed very good agreement with test data. For the CH4/O2 combustion a 7 element test case was examined. In a comparative study of several combustion simulation tools conducted by Perakis et al. [20] a good performance of Rocflam3's adiabatic flamelet model was shown. However, this study also indicates that some work on the combustion modeling of CH4/O2 remains, underlining the importance of the on-going development of adequate models.

4. Test Case Description

In Germany extensive academic research on fundamental technologies for the development of future space-transport system components under high thermal and mechanical loads is performed in the frame of the national collaborative research center Sonderforschungsbereich Transregio 40 (SFB-TRR 40) funded by the German research society (Deutsche Forschungsgemeinschaft, DFG). During the final period of the SFB-TRR 40 the generated knowledge and tools shall be applied to realistic full-scale LRE thrust chamber configurations to assess the impact of the individual research topics. To facilitate this effort ArianeGroup Ottobrunn has defined three individual thrust chamber demonstrators (TCD) that cover all relevant technologies researched within the SFB-TRR 40. As the production and test of three full-scale thrust chambers by far exceeds the available capacities of the SFB-TRR 40 these demonstrators shall remain virtual testbeds, defined to industry standard. A more detailed overview of all three demonstrators and their role within the SFB-TRR 40 is given by Eiringhaus et al. [5]. For the investigations carried out in this work only the first thrust chamber demonstrator (TCD1) is regarded.

The demonstrator TCD1 is designed as a test bed for a modern hydrogen / oxygen upper stage engine in the 100 kN thrust range. It utilizes the closed expander cycle and thus the turbo pumps are solely driven by the heated up cooling fluid and no auxiliary combustion device is needed. Hence, the heat transfer from the hot gas to the coolant side plays a vital role both under the aspect of achievable life time and under the aspect of cycle optimization. In order to achieve a sufficient enthalpy increase in the cooling channels a typical expander cycle combustion chamber exhibits an elongated cylindrical section and / or an interface of the combustion chamber and the nozzle extension at rather high aspect ratios. Both means lead to a lengthening of the cooling passages and ensure a sufficient increase of coolant enthalpy at the drawback of increasing the thrust chamber mass. As a decrease in the mass of the propulsion system trades directly with an increase in payload mass and thus performance, possibilities for thrust chamber mass minimization shall be investigated. An increased heat transfer to the fluid under the constraint of keeping the maximum structure temperature at a tolerable level allows the shortening of the combustion chamber or shifting the interface of combustion chamber and nozzle extension upstream (to lower aspect ratios) which both leads to a decreased chamber

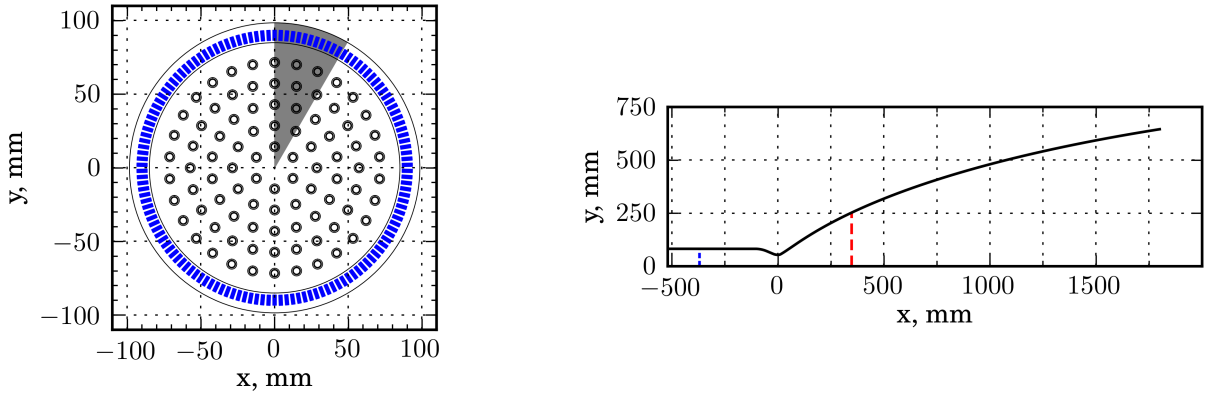

(a) Injection element pattern and cooling channel configuration of TCD1. The grey area indicates the computational domain.

(b) Hot gas wall contour of TCD1. Dashed red line: interface between combustion chamber and nozzle extension. Dashed blue line: minimum required l^* for complete combustion.

Figure 3: Geometry of TCD1

DOI: 10.13009/EUCASS2019-251

mass.

The resulting thrust chamber is designed for a nominal combustion chamber pressure p_c of 55 bar and a LOX / LH2 mixture ratio of 5.6 and thus comparable to the European Vinci [4] and the US American RL-10C [10] engine. The contour of the hot gas wall of TCD1 is illustrated in Fig. 3b. The interface between the metallic combustion chamber that is regeneratively cooled and the radiatively cooled nozzle extension manufactured from high temperature resistant ceramics at an expansion ratio $\varepsilon_{I/F}$ of 22 is indicated by the red dashed line. The dashed blue line denotes the minimum required characteristic length l^* for complete combustion as given by Huzel and Huang [9]. For the aforementioned mass optimization of the demonstrator the shortening of the cylinder towards this line is one major design goal. The divergent part of the nozzle is realized as a truncated ideal contour (TIC) free of any internal shocks [2] with an expansion ratio of ε_e of 143.2.

The combustion chamber is designed as an integral chamber with a liner from oxygen free high conductivity copper (OFHC-Cu) and a Nickel (Ni) jacket with 138 milled cooling channels. These cooling channels are routed in flow direction of the hot gas (co-flow), exhibit varying dimensions along the axis and are tailored for maximum heat pick up and minimum pressure loss as depicted in Figure 4.

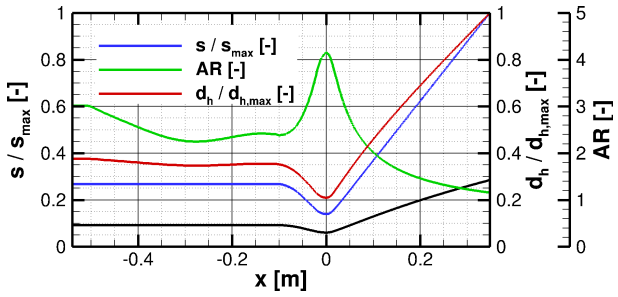

Figure 4: Dimensionless hot gas wall thickness $s/s_{\max}$, dimensionless hydraulic diameter $d_{\mathrm{h}}/d_{\mathrm{h,max}}$ and aspect ratio $AR = h_{\mathrm{ch.}}/w_{\mathrm{ch.}}$ of the cooling channels of demonstrator TCD1

The injector head of TCD1 is depicted in Fig. 3a. It features 90 shear coaxial injection elements in five concentric circles where the inner circle has six elements and in each consecutive circle six more elements are added. This way a high degree of symmetry is ensured which facilitates numerical analyses.

While being a full-scale test case the upper stage demonstrator TCD1 is still substantially smaller than a typical main stage thrust chamber. A comparison of the minimal required computational domain for a CHT analysis of different thrust chamber configurations is shown in Figure 5. From left to right a typical sub-scale combustion chamber (7-element GCH4/GOX chamber of Silvestri et al. [25]), the demonstrator TCD1 as an example for upper stage engines and a main stage demonstrator from SFB-TRR 40 are depicted. Noticeably, not only does the geometry increase in size but additionally the number of injection elements and cooling channels that have to be resolved by the model increases drastically. Hence, TCD1 lends itself to a first application of novel combustion simulation setups and tools.

5. Application of the CHT Tool

Below, the thrust chamber demonstrator TCD1 introduced in section 4 is used as a test case for the CHT method described in section 3. The numerical setup of both the combustion simulation with Rocflam3 and the structure / cooling channel analysis with Ansys CFX is presented in section 5.1. Subsequently, results of the CHT analysis are presented in section 5.2.

5.1 Numerical Model

In the following two sections a short overview of the numerical models used for the CHT analysis is given. The computational domain for both tools is a 30° segment as indicated in Figure 3a that extends from the faceplate to the nozzle extension interface at an expansion ratio $\varepsilon_{I/F}$ of 22 as illustrated by the red dashed line in Figure 3b.

5.1.1 Combustion Domain

The computations with Rocflam3 are performed on a block structured grid consisting of more than 7 million hexahedral cells as depicted in Figure 6. All walls are modeled as no-slip walls. The faceplate is assumed to be adiabatic, whereas at the perimeter of the computational domain the temperature from the Ansys CFX simulation is prescribed. The

DOI: 10.13009/EUCASS2019-251

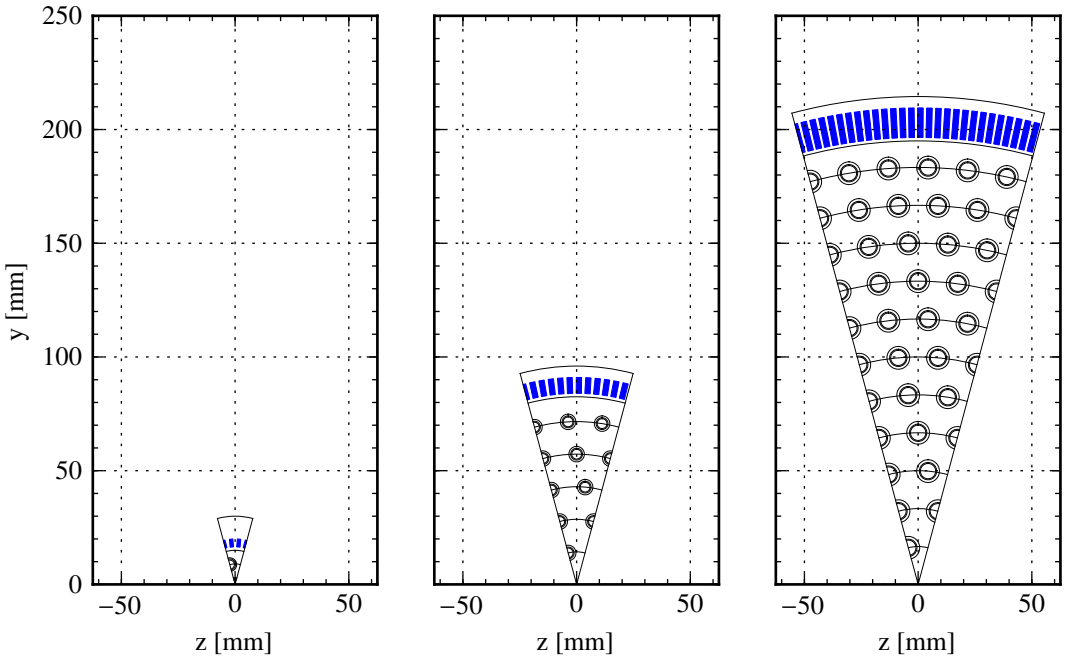

Figure 5: Comparison of typical CFD simulation domains for a sub-scale, upper stage and main stage engine.

mapping of the inlet boundary conditions as described in section 3.1 is illustrated in Figure 6b. Red areas indicate inlet boundary conditions for the hydrogen whereas blue areas indicate inlet boundary conditions for the oxygen. It can be seen that this choice of mesh topology does not allow a resolution of the individual post tip.

The hydrogen is injected with a temperature of 200 K and thus in a supercritical state. The complete fuel mass flow is injected into the domain using the above described mass flow inlet boundary condition. The oxidizer is injected with a temperature of 95 K. At a chamber pressure of about 55 bar the oxygen is hence supercritical in pressure but subcritical in temperature. Riedmann et al. [22] showed that for the injection of transcritical oxygen a combination of a mass flow inlet and the particle injection via the Lagragian module works best in Rocflam3. Thus, 80% of its mass flow are inserted as droplets whereas the remaining 20% are injected as a dense gas via the mass flow inlet.

Turbulence modeling is done with Menter's k-ω-SST model and both the turbulent Schmidt number Sc_t and the turbulent Prandtl number Pr_t are set to a value of 0.6. These values are the result of extensive parameter studies on well-instrumented sub-scale combustion chambers and are applied for all H2/O2 thrust chambers. The hot gas wall is assumed to be hydraulic smooth, thus no wall roughness is prescribed. Furthermore, the mesh resolution is chosen such that the dimensionless wall distance of the wall nearest cell y^+ is in the order of 1.

As the demonstrator TCD1 utilizes the propellant combination H2/O2 the equilibrium based tabulated chemistry model is employed.

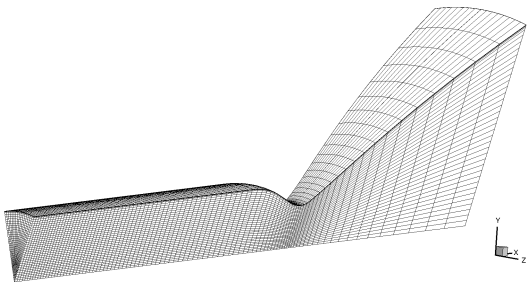

(a) Computational grid for Rocflam3 3D simulations (every 5th grid line shown)

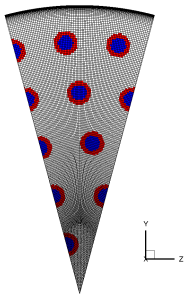

(b) Injector mapping on regular grid for Rocflam3 3D simulations

Figure 6: Grid strategies for Rocflam3 3D computations

DOI: 10.13009/EUCASS2019-251

5.1.2 Structure and Coolant Domain

For the simulation of the wall structure and the coolant flow a 30° segment matching the combustion domain is analyzed. This segment includes 11.5 cooling channels. A block structured computational grid is used that contains 7.9 million cells in the domain of the copper liner and fins, 6.1 million cells in the domain of the outer nickel shell and 39.2 million cells in the fluid domain.

For all cooling channels a static inlet temperature of 35 K and a static outlet pressure of 175 bar is prescribed. A total mass flow of 271 g/s is set for the combined cooling channel inlet surfaces which permits varying mass flow rates per cooling channel dependent on the individual pressure loss that is affected by the coolant heat up. At the inner perimeter surface the heat flux from the Rocflam3 combustion simulation is prescribed. All other solid surfaces that are not in contact to the coolant are assumed to be adiabatic.

For both the nickel and the OFHC-Cu temperature dependent data for the thermal conductivity are implemented. Also, tabulated real gas properties of parahydrogen are used.

Turbulence modeling is done with Menter's SST model. For the cooling channel walls a sand grain roughness compliant to milled channels is set. In the fluid domain a dimensionless wall distance y^+ in the order of 1 is ensured.

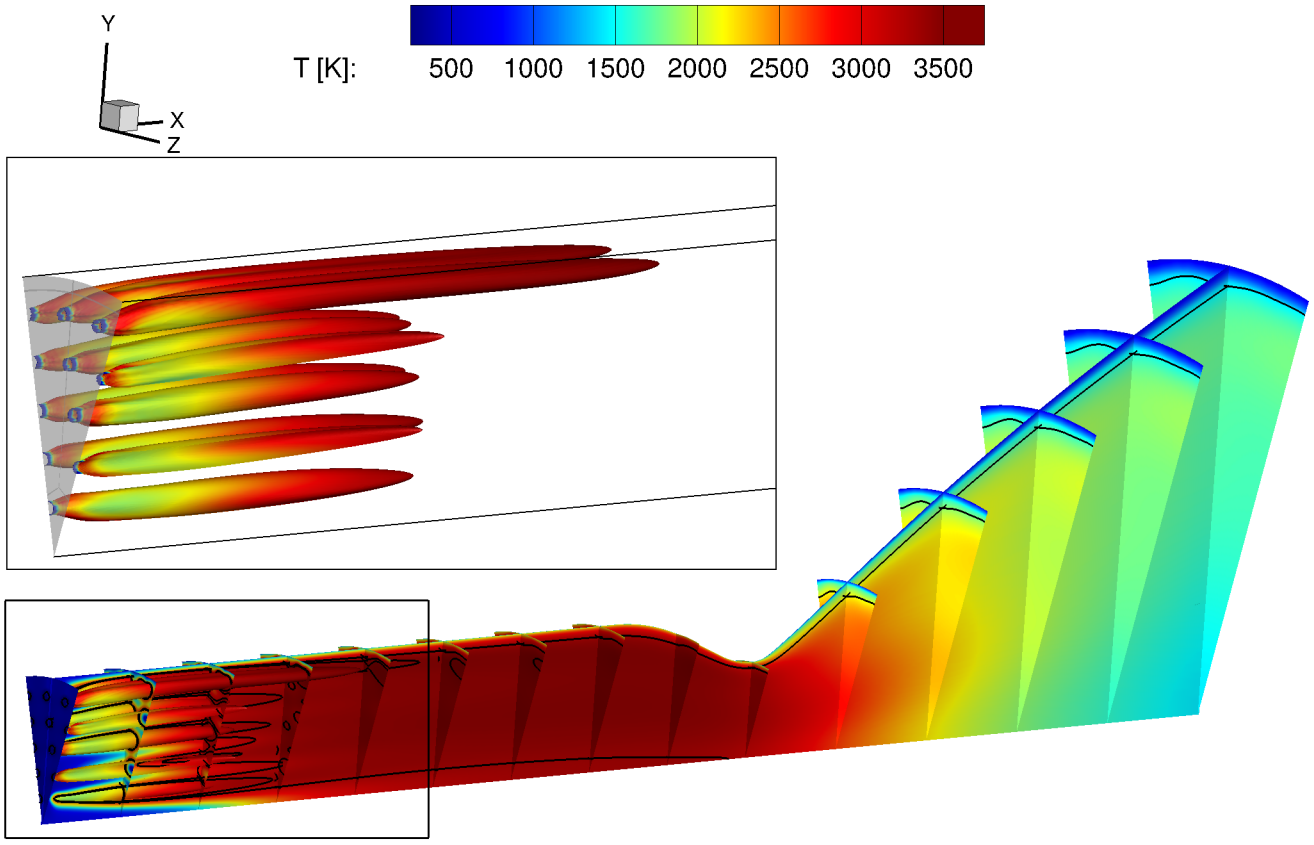

Figure 7: Slices at selected positions and iso-planes of stoichiometric mixture fraction colored by the hot gas temperature. Black lines denote deviations of ±10% of the local ROF from the global ROF. The zoom shows a detailed view of the stoichiometric mixture fraction iso-planes.

5.2 Results

Convergence of both the wall heat flux computed by Rocflam3 and the wall temperature computed by Ansys CFX was achieved after several coupling steps.

The resulting temperature field of the hot gas is depicted in Figure 7. The main reaction zone is indicated by iso-planes of stoichiometric mixture fraction. The black lines denote deviations of ±10% of the local ROF from the global ROF of 5.6. An elongated reaction zone can be observed for the outermost row. This is attributed to the extraction of heat towards the cooled combustion chamber wall. Both the temperature field and the ROF show a good

DOI: 10.13009/EUCASS2019-251

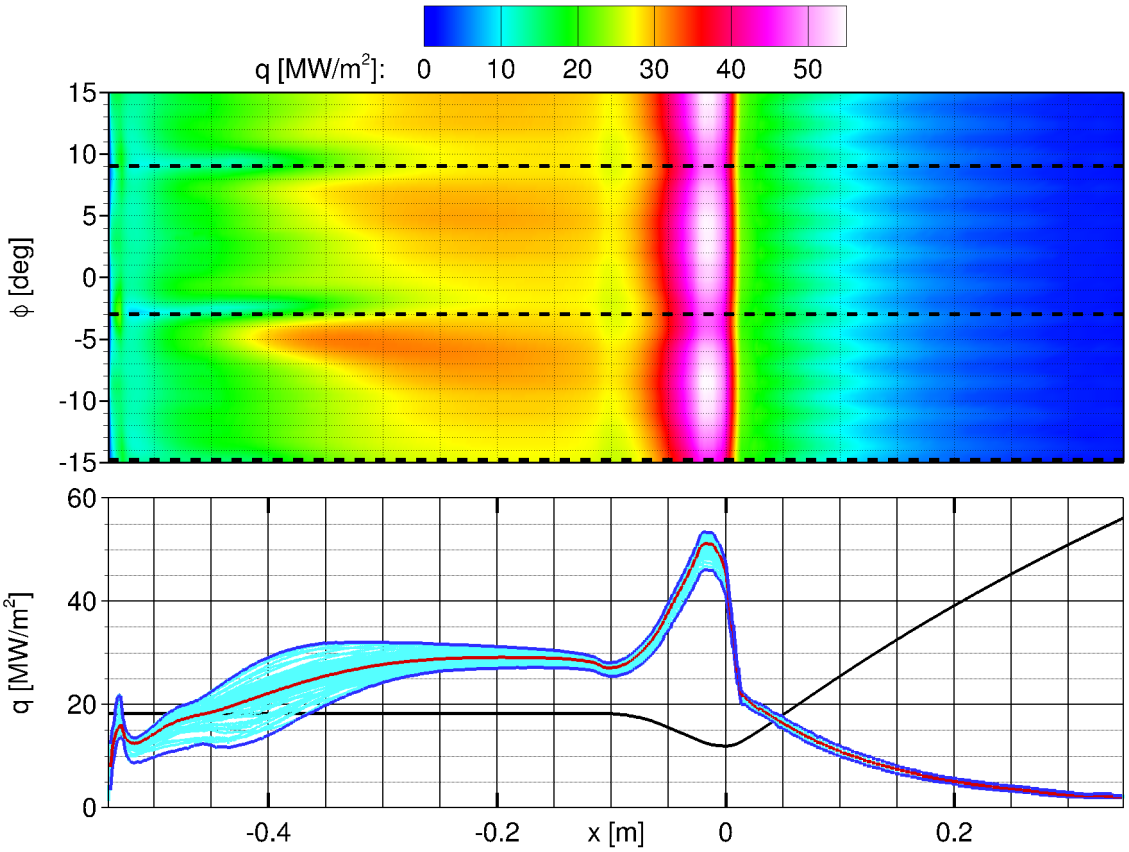

Figure 8: Wall heat flux axial profile (bottom) and wall map in a x-ϕ-coordinate frame (top).

mixing downstream ca. 50% of the cylinder length with slightly fuel rich zones near the wall. This is favorable as it prevents blanching effects which occur when the copper liner comes into contact with high temperature oxygen. Due to the good mixing which is promoted by the high characteristic length of 1.2 m a high combustion efficiency can be expected.

The resulting heat flux at the combustion chamber wall is illustrated in Figure 8. The bottom graph of Figure 8 shows the axial profile of the wall heat flux. The dark blue lines denote the circumferential minimum and maximum value of the heat flux whereas the circumferential mean value is given by the red line. An initial local maximum near the faceplate can be identified that results from a recirculation. Downstream, as the combustion reaction progresses, the overall level of the heat flux increases along with its circumferential variation. At about $x = -0.25$ m the heat flux reaches a plateau and its variation is decreased. The global maximum can be observed slightly upstream of the throat where again the circumferential variation is increased. Downstream of the throat the heat flux rapidly decreases as the hot gas is expanded.

The top graph of Figure 8 illustrates the local wall heat flux in a view on the combustion chamber wall. For the ordinate the local wall angle $\phi = \arctan(z/y)$ is used as geometrical coordinate. The dashed lines denote the azimuthal position of the injection elements of the outermost row at $-15°$, $-3°$ and $9°$. It can be seen that in the wake of the injection elements the heat flux level is decreased whereas at the positions between the injection elements the heat flux is intensified. Furthermore, in the supersonic region downstream of about $x = 0.1$ m an additional circumferential variation of the wall heat flux can be observed that is linked to the azimuthal positions of the cooling channels.

The resulting hot gas wall temperature is shown in Figure 9. The bottom graph of Figure 9 shows the axial profile of the wall temperature. The dark blue lines denote the circumferential minimum and maximum value of the temperature whereas its circumferential mean value is given by the red line. Near the faceplate the wall temperature reaches very low values. One impacting factor is the co-flow routing of the coolant medium and its very low inlet temperature of only 35 K. Additionally, on the hot gas side a fuel rich recirculation zone is established above the outer most element row that impedes the heat transfer. The general axial trend of the wall temperature follows that of the wall heat flux exhibiting a plateau in the cylinder, a local minimum at the onset of the convergence, a global maximum

DOI: 10.13009/EUCASS2019-251

in the throat and a subsequent steep decrease.

The top graph of Figure 9 shows the wall temperature in a x-ϕ-coordinate frame. The dashed lines denote the azimuthal position of the injection elements of the outermost row at $-15°$, $-3°$ and $9°$. Concerning the influence of the outermost injection elements on the wall temperature profile similar observations as for the heat flux can be made. However, the influence of the individual cooling channels on the wall temperature is more pronounced and especially well visible near $x = -0.1$ m.

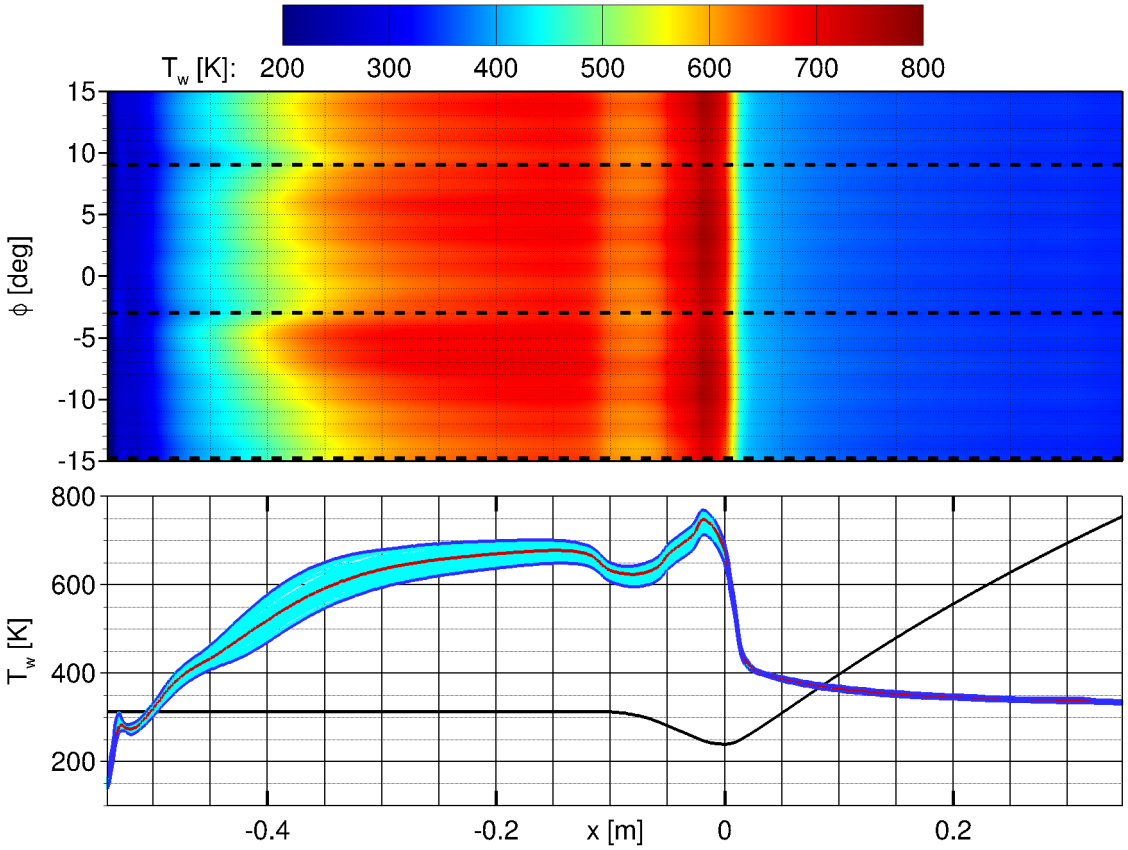

Figure 9: Wall temperature axial profile (bottom) and wall map in a x-ϕ-coordinate frame (top).

For strongly cooled rocket engines such as the examined TCD1 water can condense at the hot gas wall which can impact both engine performance and heat release. Figure 10 illustrates the occurrence of condensation of water. The bottom graph of Figure 10 shows the axial profile of the liquid water mass fraction averaged over the complete cross section. Noticeably, the total amount of liquid water is very small as it only occurs in the vicinity of strongly cooled walls. A relatively high mass fraction of liquid water can be observed near the faceplate as the wall temperature reaches its global minimum in this area. Furthermore, as the pressure rapidly decreases downstream of the throat additional condensation occurs in the supersonic part of the combustion chamber.

The top graph of Figure 10 depicts the mass fraction of liquid water in the wall nearest cell in a x-ϕ-coordinate frame. The dashed lines denote the azimuthal position of the injection elements of the outermost row at $-15°$, $-3°$ and $9°$. As can be seen the local mass fractions of liquid water can reach more than 50% at the wall. Additionally, the localization of the liquid water directly above the injection element in the recirculation zone and directly below the cooling channels in the supersonic regime can be noticed. The condensation downstream the throat also explains the observed striation of the wall heat flux in Figure 8 as the latent heat of the water is released leading to a locally increased wall heat flux.

The evaluation of the coolant simulation shows a mean pressure drop in the cooling channels of 5.1 bar and a coolant outlet bulk temperature of 222.7 K, i.e. a coolant temperature increase ΔT of 187.7 K. Due to the non-symmetric heating of the individual cooling channels, a slight variation of the coolant mass flow per cooling channel and the coolant exit temperature can be observed. However, both the variation of the mass flow rate and the variation

DOI: 10.13009/EUCASS2019-251

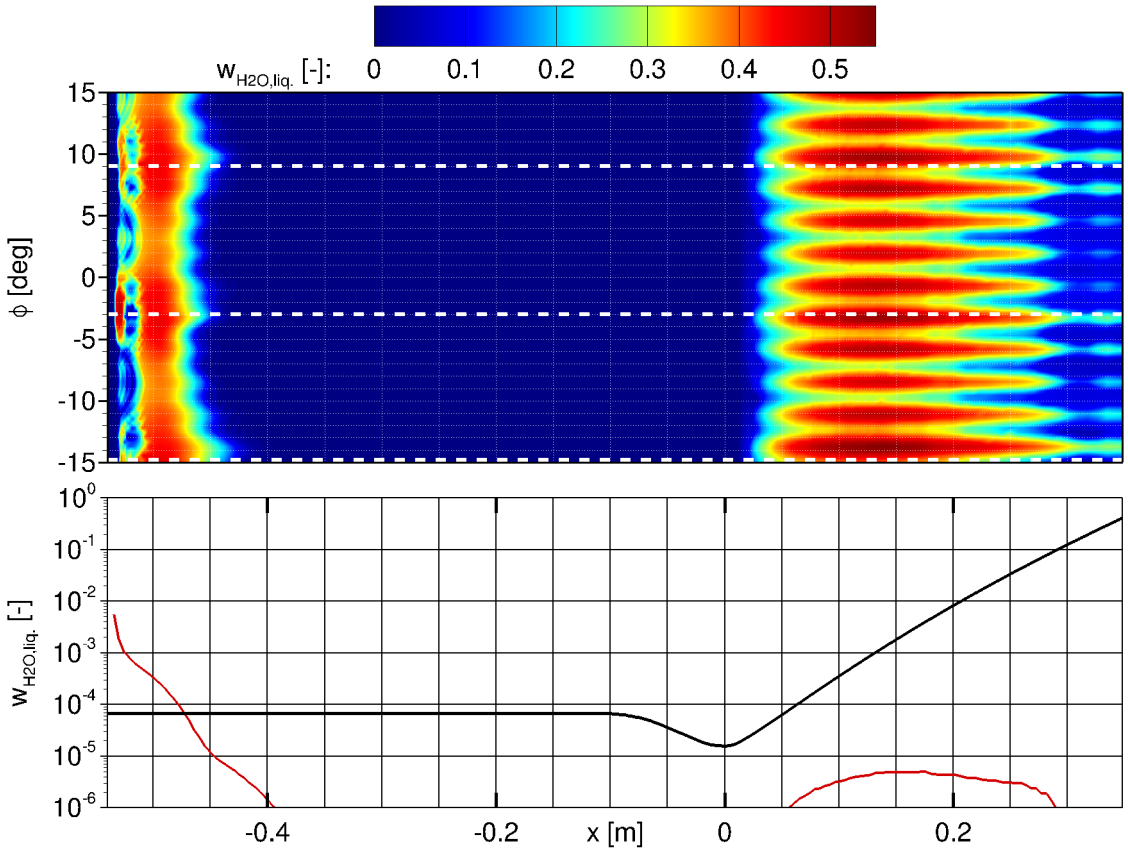

Figure 10: Mass fraction of liquid water in the wall nearest cell (top) and its axial profile (bottom).

of the outlet bulk temperature are below ±1%.

The strong radial temperature gradient in the combustion chamber wall structure can be recognized when Figure 11 is considered. The temperature profile at the cooling channel lower wall still resembles that of the hot gas wall. It also shows a similar bandwidth of variation. At the cooling channel top wall and the interface of the OFHC-Cu liner and the Ni shell (i.e. at the same radial position in the fin) the temperature profile is flattened and shows a decreased circumferential variation. Finally, at the outer combustion chamber wall only a rather small temperature variation can be observed. This indicates that an experimental verification of the circumferential hot gas stratification solely based on surface temperature measurements on the outer wall will not be possible. Instead, direct measurement of the wall temperature using flush mounted thermocouples at different circumferential positions is recommend.

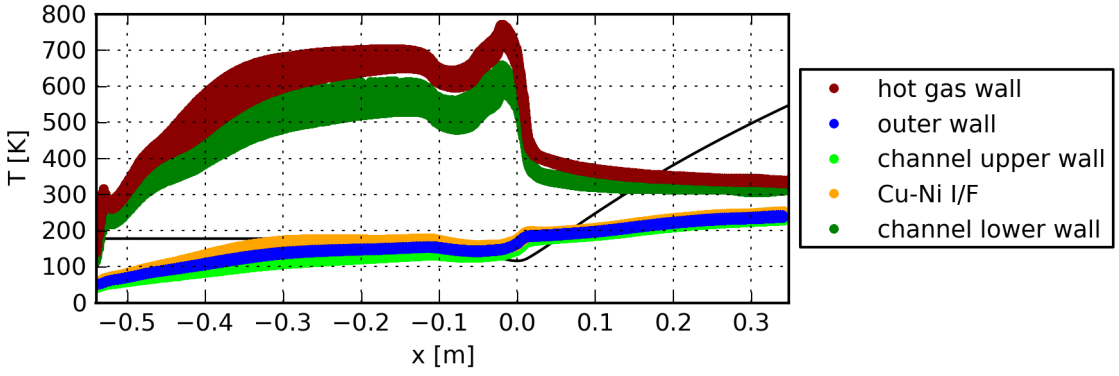

Figure 11: Solid temperatures at different radial positions.

DOI: 10.13009/EUCASS2019-251

6. Conclusion & Outlook

A method for a fully-resolved 3D conjugate heat transfer analysis of LRE thrust chambers was introduced. First results for a full-scale upper stage combustion chamber were presented showing the capabilities of such a tool. Noticeably, the wall temperature and wall heat flux each show a significant variation in circumferential direction and localized 3D phenomena like the condensation beneath individual cooling channels are resolved. Both the outermost row of injection elements and the individual cooling channels show their footprint in the hot gas wall temperature distribution. However, first investigations show that the validation of such a tool with experimental data will be difficult as neither coolant exit conditions nor outer wall surface temperatures (mostly the only measurements that are available in full-scale configurations) show sufficient magnitude of circumferential variation.

To further assess the necessity of these computational costly analyses detailed comparison to lower order tools will be performed with special focus on performance prediction, coolant pressure drop and temperature increase and maximum wall temperature. Additionally, the impact of the hot gas wall temperature stratification on structural integrity and especially life predictions will be analyzed. With its capabilities the presented CHT tool also offers the chance to perform detailed numerical investigation of the impact of the injection pattern on the heat flux variation. Here, the impact of individual rows, the element-wall distance, a possible decrease of the circumferential variation by a gaseous fuel film and the effect of patterns with a strongly decreased number of high mass flow elements are of interest.

7. Acknowledgment

Part of this work was performed within the National technology program TARES 2020. This program is sponsored by the German Space Agency, DLR Bonn, under contract No. 50RL1710. Cooperation within the SFB-TRR 40 is gratefully acknowledged.

References

[1] B. Abramzon and W. A. Sirignano. Droplet Vaporization Model for Spray Combustion Calculations. In *AIAA 26th Aerospace Sciences Meeting*, Reno, Nevada, USA, 1988.

[2] J. Ahlberg, S. Hamilton, D. Migdal, and E. Nilson. Truncated perfect nozzles in optimum nozzle design. *ARS Journal*, 31(5):614–620, Mai 1961.

[3] B. Aupoix. Wall Roughnes Modelling with k-omega SST Model. In *10th International ERCOFTAC Symposium on Engineering Turbulence Modelling and Measurements*, 2014.

[4] S. Durteste. A Transient Model of the VINCI Cryogenic Upper Stage Rocket Engine. In *43rd AIAA/ASME/SAE/ASEE Joint Propulsion Conference & Exhibit*, Cincinnati, OH, July 2007.

[5] D. Eiringhaus, H. Riedmann, O. Knab, and O. Haidn. Full-Scale Virtual Thrust Chamber Demonstrators as Numerical Testbeds within SFB-TRR 40. In *54th AIAA/SAE/ASEE Joint Propulsion Conference*, Cincinnati, OH, USA, 2018.

[6] M. Frey, T. Aichner, J. Görgen, B. Ivancic, B. Kniesner, and O. Knab. Modeling of Rocket Combustion Devices. In *10th AIAA/ASME Joint Thermophysics and Heat Transfer Conference*, Chicago, Illinois, June/July 2010.

[7] A. Fröhlich, M. Popp, G. Schmidt, and D. Thelemann. Heat Transfer Characteristics of H2/O2 - Combustion Chambers. In *29th AIAA/SAE/ASME/ASEE Joint Propulsion Conference*, 1993.

[8] Th. Fuhrmann, B. Mewes, F. Dengra-Moya, G. Kroupa, K. Lindblad, and P. Batenburg. FLPP ETID: Approaching Hot-Fire Tests of Future European Expander Technologies. In *Space Propulsion Conference 2018*, Seville, Spain, May 2018.

[9] D. K. Huzel and D. H. Huang. *Modern Engineering for Design of Liquid-Propellant Rocket Engines*. AIAA, 1992.

[10] D. Jones. Cryogenic Propulsion Stage. `https://ntrs.nasa.gov/archive/nasa/casi.ntrs.nasa.gov/20110015783.pdf`, 2016. Accessed: 13.05.2019.

DOI: 10.13009/EUCASS2019-251

[11] O. Knab, D. Preclik, and D. Estublier. Flow Field Prediction within Liquid Film Cooled Combustion Chambers of Storable Bi-Propellant Rocket Engines. In *34th AIAA/ASME/SAE/ASEE Joint Propulsion Conference & Exhibit*, Cleveland, OH, USA, July 1998.

[12] B. E. Launder and B. I. Sharma. Applications of the Energy-Dissipation Model Turbulence to the Calculation of Flow near a Spinning Disc. *Letters in Heat and Mass Transfer*, 1:131–138, 1974.

[13] E.W. Lemmon, M.L. Huber, and M.O. McLinden. *NIST Standard Reference Database 23: Reference Fluid Thermodynamic and Transport Properties - REFPROP, Version 8.0*. National Institute of Standards and Technology, Gaithersburg, 2008.

[14] C. Mäding, D. Wiedmann, K Quering, and O. Knab. Improved Heat Transfer Prediction Engineering Capabilities for Rocket Thrust Chamber Layout. In *3rd EUCASS*, 2009.

[15] B.J. McBride and S. Gordon. *Computer Program for Calculation of Complex Chemical Equilibrium Compositions and Applications: I. Analysis*. NASA Reference Publication 1311, Lewis Research Center, Cleveland, Ohio, USA, 1994.

[16] B.J. McBride and S. Gordon. *Computer Program for Calculation of Complex Chemical Equilibrium Compositions and Applications: II. User Manual and Program Description*. NASA Reference Publication 1311, Lewis Research Center, Cleveland, Ohio, USA, 1996.

[17] F. R. Menter. Two-Equation Eddy-Viscosity Turbulence Models for Engineering Applications. *AIAA Journal*, 32(8):1598–1605, August 1994.

[18] H. Negishi, Y. Daimon, H. Kawashima, and N. Yamanishi. Conjugated Combustion and Heat Transfer Modeling for Full-Scale Regeneratively Cooled Thrust Chambers. In *49th AIAA/ASME/SAE/ASEE Joint Propulsion Conference*, San Jose, CA, USA, July 2013.

[19] S. V. Patankar and D. B. Spalding. A Calculation Procedure for Heat, Mass and Momentum Transfer in Three-Dimensional Parabolic Flows. *International Journal of Heat and Mass Transfer*, 15(10):1787–1806, October 1972.

[20] N. Perakis, O. J. Haidn, D. Eiringhaus, D. Rahn, S. Zhang, Y. Daimon, S. Karl, and T. Horchler. Qualitative and Quantitative Comparison of RANS Simulation Results for a 7-Element GOX/GCH4 Rocket Combustor. In *54th AIAA/SAE/ASEE Joint Propulsion Conference*, Cincinnati, OH, USA, July 2018.

[21] D. Rahn, H. Riedmann, R. Behr, and O. Haidn. Non-adiabatic flamelet modeling for the numerical simulation of methane combustion in rocket thrust chambers. In *54th AIAA/SAE/ASEE Joint Propulsion Conference*, Cincinnati, OH, USA, July 2018.

[22] H. Riedmann, B. Kniesner, M. Frey, and C.-D. Munz. 3D Modeling of Spray Combustion and Flow in a 40kN H2/O2 Subscale Rocket Thrust Chamber. In *Space Propulsion 2014*, 2014.

[23] W. Rodi. Experience with Two-Layer Models Combining the k-ε Model with a One-Equation Model Near the Wall. In *29th Aerospace Sciences Meeting*, Reno, Nevada, 1991.

[24] A. Sharma, K. A. Deepak, J. C. Pisharady, and S. Sunil Kumar. Numerical Analysis of Combustion and Regenerative Cooling in LOX-Methane Rocket Engine. In *68th International Astronautical Congress (IAC)*, Adelaide, Australia, September 2017.

[25] S. Silvestri, M.P. Celano, G. Schlieben, and O.J. Haidn. Characterization of a Multi-Injector GOX-GCH4 Combustion Chamber. In *52nd AIAA/SAE/ASEE Joint Propulsion Conference*, Salt Lake City, Utah, July 2016.

[26] P. Simontacchi, E. Edeline, R. Blasi, S. Sagnier, N. Ravier, A. Espinosa-Ramos, and J. Breteau. Prometheus: Precursor of New Low-Cost Rocket Engine Family. In *Space Propulsion Conference 2018*, Sevilla, Spain, May 2018.

[27] H. Stone. Iterative Solution of Implict Approximation of Multidimensional Partial Differential Equation. *SIAM Journal on Numerical Analysis*, pages 530–558, 1968.

[28] D. Wilcox. Formulation of the k-ω turbulence model revisited. In *45th AIAA Aerospace Sciences Meeting and Exhibit*, Reno, Nevada, January 2007.